Constructing Nickel Sulfide Heterojunction by W-doping-induced Structural Transition for Enhanced Oxygen Evolution

Ziqian Xue,[+] Yawen Liu, [+] Qinglin Liu, Yawei Zhang, Meng Yu, Qianwei Liang, Jianqiang Hu and Guangqin Li**

Dr. Z. Xue, Q. Liu, Y. Zhang, Prof. G. Li
MOE Laboratory of Bioinorganic and Synthetic Chemistry
Lehn Institute of Functional Materials
School of Chemistry
Sun Yat-Sen University
Guangzhou, 510275, P. R. China
E-mail: liguangqin@mail.sysu.edu.cn

Y. Liu, Dr. Y. Meng, Dr. Q. Liang, Prof. J. Hu
College of Chemistry and Chemical Engineering
South China University of Technology
Guangzhou, 510640, P. R. China
E-mail: jqhusc@scut.edu.cn

1. Experimental Section

1.1 Chemicals

Thioacetamide (TAA, CH_3CSNH_2, AR, 99%), sodium tungstate dihydrate ($Na_2WO_4·2H_2O$, ACS, 99.0-101.0%), Nickel(II) acetylacetonate ($C_{10}H_{14}NiO_4·2H_2O$, AR, 99%), Thiourea (CH_4N_2S, AR, 99%), PVP (Polyvinylpyrrolidone, K30), Monoethanolamine (C_2H_7NO, AR), Diethanolamine ($C_4H_{11}NO_2$, AR), KOH and commercial RuO_2 were purchased from Aladdin (Shanghai, China).

1.2 Synthesis of W-Ni_3S_2/Ni_7S_6.

The W-Ni_3S_2/Ni_7S_6 nanorod array was synthesized by a simple hydrothermal method. Firstly, 250 mg thioacetamide (TAA, CH_3CSNH_2), 1.5 mmol sodium tungstate dihydrate ($Na_2WO_4·2H_2O$) and 40 mg PVP were dissolved in 60 mL deionized water, continuous stirring for 20 min. Meanwhile, a piece of Ni foam (2×3 cm^2) was cleaned by ultrasonic treatment with 3 M HCl solution, ethanol, and deionized water for 20 min each. Secondly, Ni foam was immersed into the prepared

solution and heating the solution at 160℃ for 12 h in a sealed autoclave. Finally, the hydrothermal product was washed with deionized water and dried in air to obtain the W-Ni_3S_2/Ni_7S_6 nanorod arrays catalyst. The loading weights of W-Ni_3S_2/Ni_7S_6 on Ni foam were approximately 2.5 mg·cm^{-1}.

1.3 Synthesis of W-Ni_3S_2.

For preparing the W-Ni_3S_2 nanorod arrays, 250 mg thioacetamide (TAA, CH_3CSNH_2), 35 mg sodium tungstate dihydrate ($Na_2WO_4·2H_2O$) and 40 mg PVP were dissolved in 60 mL deionized water, continuous stirring for 20 min. Meanwhile, a piece of Ni foam (2×3 cm^2) was cleaned by ultrasonic treatment with 3 M HCl solution, ethanol, and deionized water for 20 minutes each. Then, Ni foam was immersed into the prepared solution and heating the solution at 160℃ for 12 h in a sealed autoclave. Finally, the hydrothermal product was washed with deionized water and dried in air to obtain the W-Ni_3S_2 nanorod arrays. The loading weights of The W-Ni_3S_2 on Ni foam were approximately 2.3 mg·cm^{-1}.

1.4 Synthesis of Ni_3S_2

For preparing the Ni_3S_2, 250 mg thioacetamide (TAA, CH_3CSNH_2) and 40 mg PVP were dissolved in 60 mL deionized water, continuous stirring for 20 min. Meanwhile, a piece of Ni foam (2×3 cm^2) was cleaned by ultrasonic treatment with 3 M HCl solution, ethanol, and deionized water for 20 minutes each. Then, Ni foam was immersed into the prepared solution and heating the solution at 160℃ for 12 h in a sealed autoclave. Finally, the hydrothermal product was washed with deionized water and dried in air to obtain the Ni_3S_2 catalyst supported on Ni foam. The loading weights of Ni_3S_2 on Ni foam were approximately 2.2 mg·cm^{-1}.

1.5 Synthesis of Ni_7S_6

For preparing the Ni_7S_6, 0.0617 g nickel (ii) acetylacetonate, 0.0213 g thiourea, and 100 mg PVP were dispersed in the mixture of H_2O (2.0 mL), ethanolamine (6.0 mL), and diethanolamine (2.0 mL). The above mixtures were stirred for 60 minutes and heating the solution at 160℃ for 12 h in a sealed autoclave. The loading amount

of Ni_7S_6 catalyst on the Ni foam is about 2.5 mg·cm^{-2}, which is the same loading mass with our catalyst.

1.6 Preparation of RuO_2 supported on Ni foam.

The RuO_2 supported on Ni foam was prepared with the help of Nafion (5%) solution. The commercial RuO_2 (10 mg) was dispersed into a mixture of 980 μL ethanol and 20 μL Nafion solution. Then, the mixture was ultrasonicated for 30 min to obtain a homogeneous dispersion. Finally, the dispersed solution was loaded onto nickel foam, followed by the dry in air at room temperature. The loading amount of RuO_2 catalyst on the Ni foam is about 2.5 mg·cm^{-2}, which is the same loading mass with our catalyst.

1.7 Material characterizations

Characterization X-ray diffraction patterns were performed on the Rigaku SmartLab diffractometer with Cu Kα X-ray source (λ=1.540598 Å). The field-emission scanning electron microscopy (FE-SEM) images were recorded on a Hitachi SU8010 system. Transmission electron microscopy (TEM) images were collected by a JEM-1400Plus transmission electron microscopy. Scanning transmission electron microscopy (STEM) and EDS mapping images were measured on a JEOL JEM-ARM 200F equipped with an energy dispersive X-ray spectrometer, operating at 200 kV. X-ray photoelectron spectra (XPS) tests were carried out on a VG Scientific ESCALAB 250 instrument.

1.8 Electrochemical measurements

The electrochemical tests were conducted on the CHI 760E via a general three-electrode system in 1 M KOH electrolyte at room temperature. For detail, platinum plate electrode as the counter electrode and Ag/AgCl (KCl saturated) electrode as the reference electrode. Linear sweep voltammetry (LSV) curves were measured at a scan rate of 2 mV·s^{-1}. The obtained potential in the LSV polarization curves was corrected for 95% iR losses to minimize the influence of ohmic resistance. The measured potentials versus the reversible hydrogen electrode (RHE) were converted according to the Nernst equation ($E_{RHE}=E_{Ag/AgCl}$ + 0.197 +0.059 ×pH)[1]. The double-layer capacitance (C_{dl}) at different scanning rates was measured by cyclic voltammetry (CV)

within a potential range of 1.036-1.136 V vs. RHE to investigate the electrochemical active surface area (ECSA). Electrochemical impedance spectra (EIS) were measured with 5 mV amplitude in the frequency of 0.1 Hz ~100 kHz at 1.55 V vs. RHE. The turnover frequency (TOF) was calculated by the equation: TOF = (J×A) / (4×F×m), where J is the current density (A cm^{-2}) at an overpotential of 300 mV, A and m represent the area of the electrode and the number of moles of the active materials, F represents Faraday constant (96,485 C mol^{-1}).

2. Supplementary figures

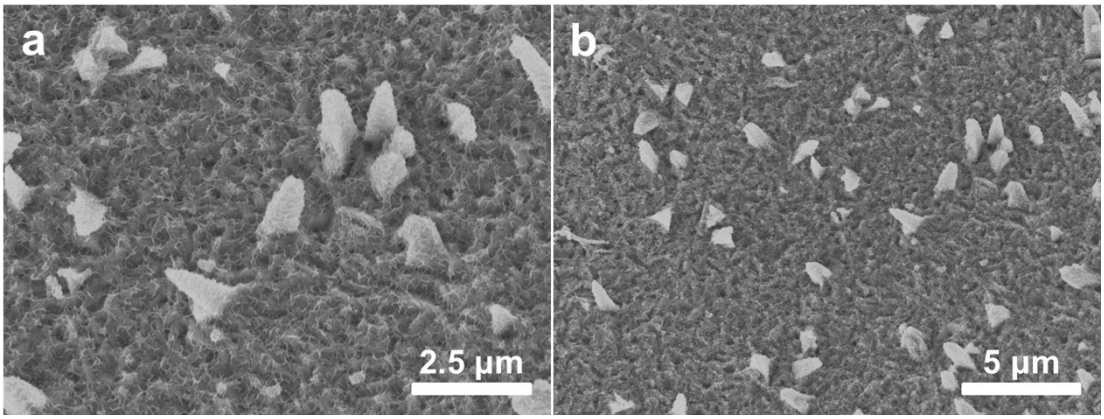

Figure S1. SEM images of Ni_3S_2.

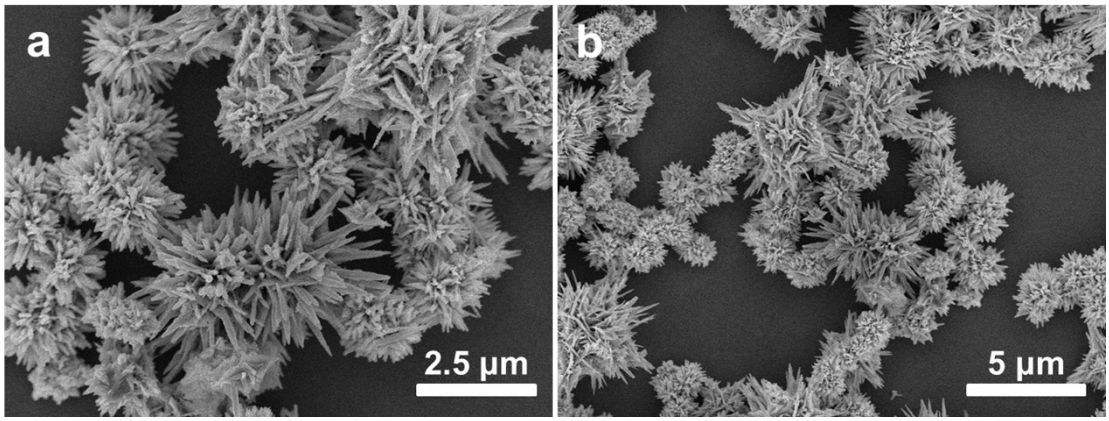

Figure S2. SEM images of Ni_7S_6.

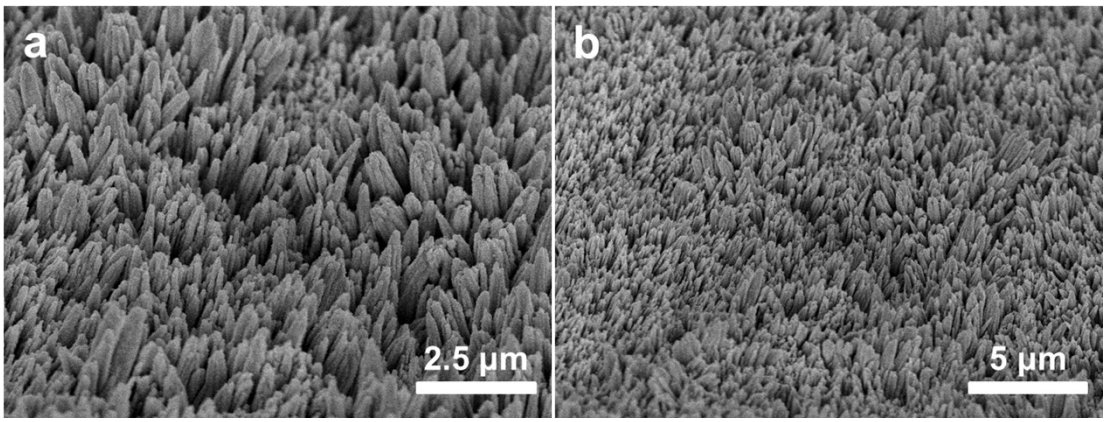

Figure S3. SEM images of W-Ni_3S_2.

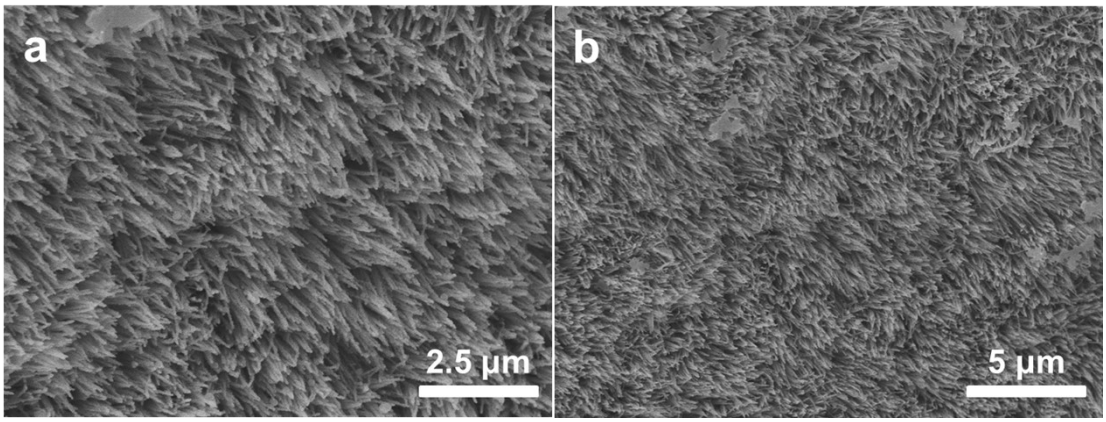

Figure S4. SEM images of W-Ni_3S_2/Ni_7S_6.

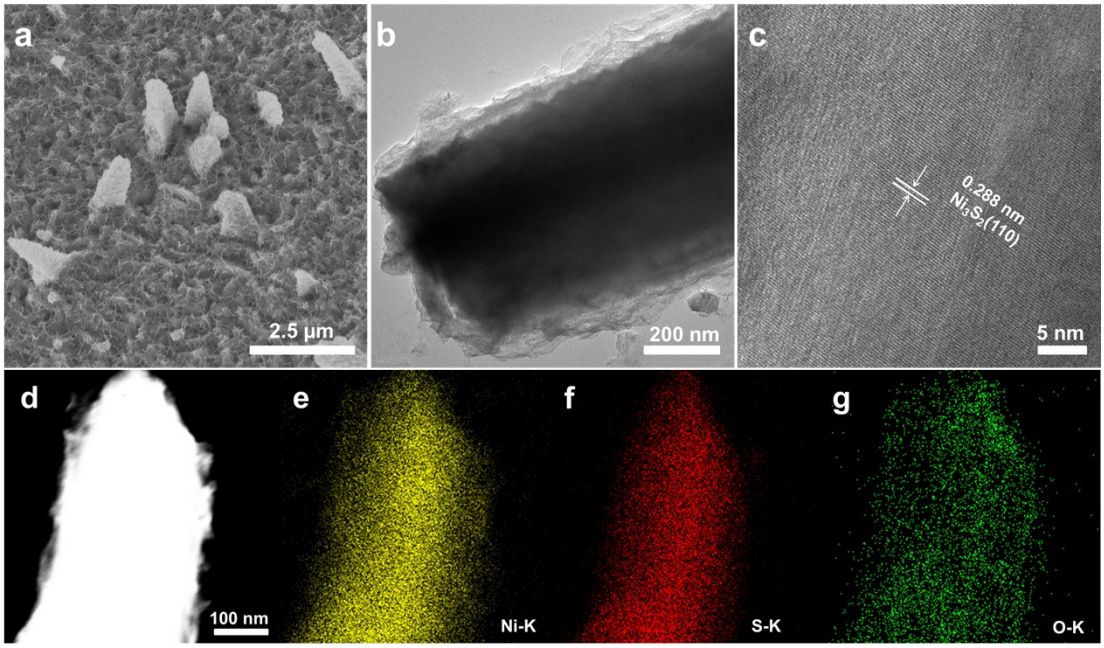

Figure S5. a) FESEM, b) TEM, c) HRTEM images of the Ni_3S_2. d–g) HAADF-STEM image and STEM-EDS mappings of Ni_3S_2.

Table S1. The molar ratio of Ni/W in different catalysts

catalyst	Mass%		Atom%	
	Ni	W	Ni	W
Ni_3S_2	100.00	0	100	0
W- Ni_3S_2	99.32	0.68	99.78	0.22
W- Ni_3S_2/Ni_7S_6	87.62	12.38	95.68	4.32

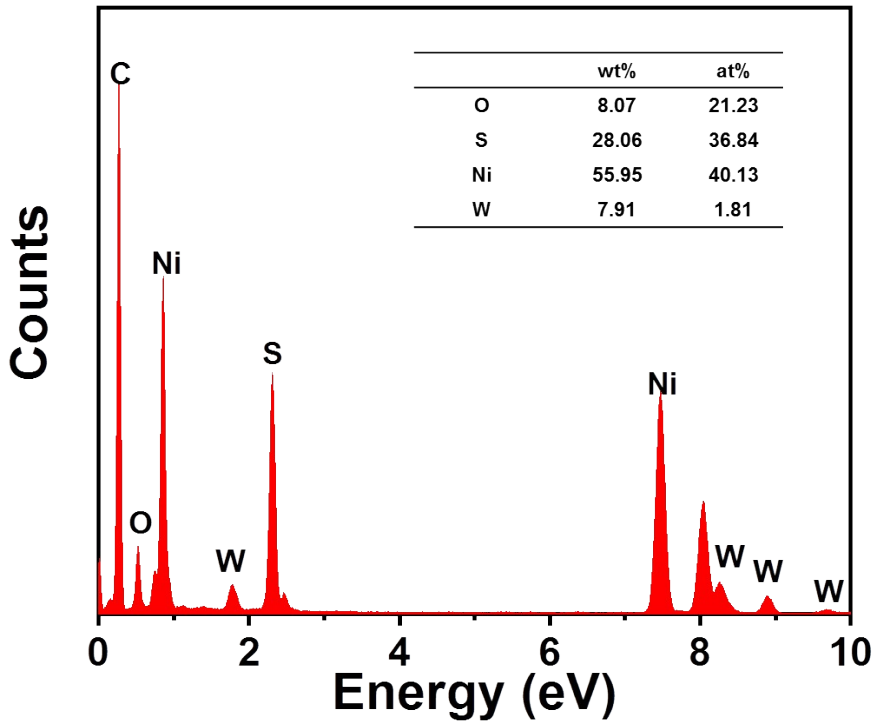

	wt%	at%
O	8.07	21.23
S	28.06	36.84
Ni	55.95	40.13
W	7.91	1.81

Figure S6. Energy dispersive X-ray (EDX) spectrum of W-Ni_3S_2/Ni_7S_6.

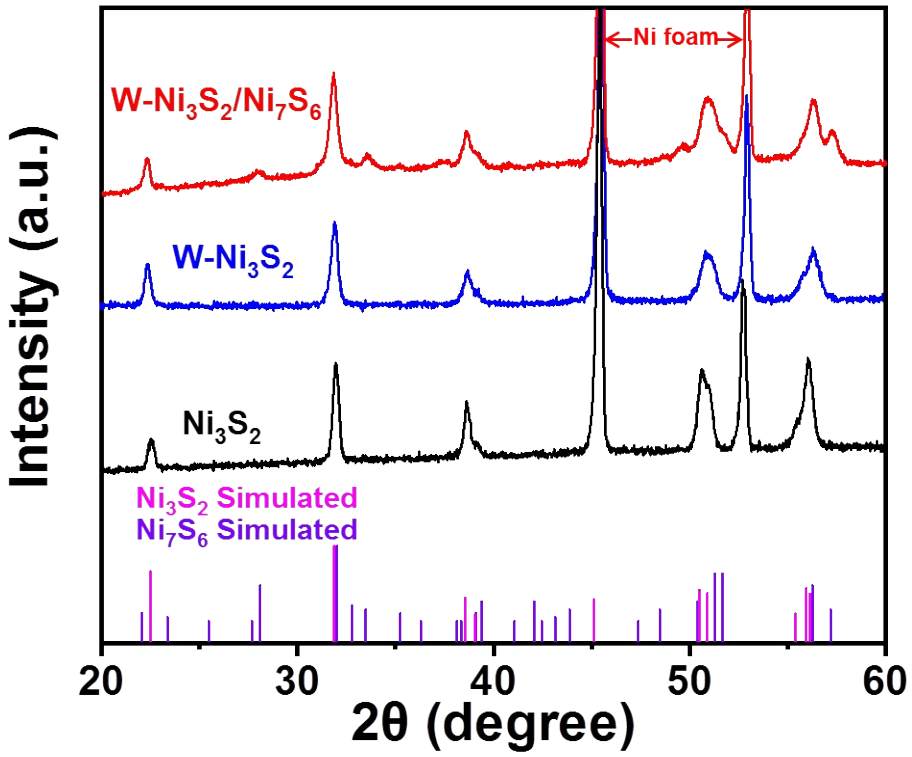

Figure S7. XRD of Ni_3S_2, W-Ni_3S_2 and W-Ni_3S_2/Ni_7S_6.

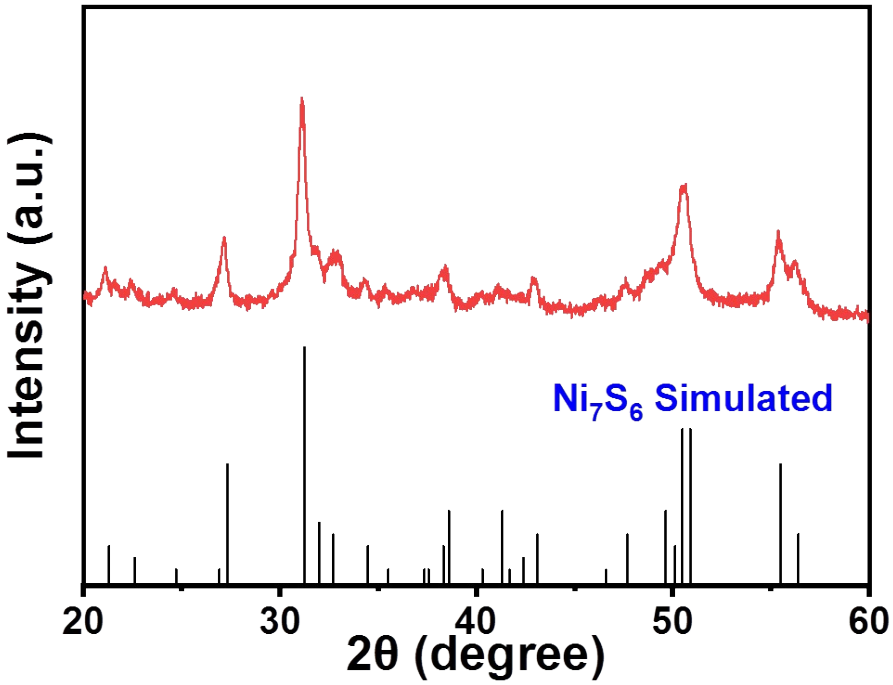

Figure S8. XRD of Ni_7S_6.

Table S2. Comparisons of OER activity of art non-noble-metal electrocatalysts.

catalyst	Electrolyte	Overpotential (mV)	Tafel slope (mV dec^{-1})	Substrates	Reference
W-Ni_3S_2/Ni_7S_6	1.0 M KOH	η_{100}=202 η_{200}=285	27.9	Ni foam	This work
Ni_3S_2	1.0 M KOH	η_{10}=324	72.1	Ni foam	[2]
$Fe_{0.9}Ni_{2.1}S_2$@NF	1.0 M KOH	η_{100}=252	64	Ni foam	[3]
CoMoNiS-NF-31	1.0 M KOH	η_{100}=260	85	Ni foam	[4]
Mo-Ni_3S_2/Ni_xS_y/NF	1.0 M KOH	η_{50}=238	60.6	Ni foam	[5]
3D Se-$(NiCo)S_x(OH)_x$	1.0 M KOH	η_{10}=155	33.9	Ni foam	[6]
Ni_3S_2 NTFs	1.0 M NaOH	η_{100}=330	101.2	Ni foil	[7]
$CoMoS_4$/Ni_3S_2	1.0 M KOH	η_{10}=200	63	-	[8]
FeMOFs-SO_3	1.0 M KOH	η_{10}=218 η_{500}=298 η_{1000}=330	36.2	-	[9]
$(Co_{0.85}Fe_{0.15})_9S_8$	1.0 M KOH	η_{10}=255	49	-	[10]
Ni_3S_2@$Co(OH)_2$	1.0 M KOH	η_{10}=290	90.7	Ni foam	[11]
Ni_3S_2@graphite foam	1.0 M KOH	η_{10}=240	62.4	Ni foam	[12]
Co_9S_8-Ni_3S_2 nanoarrays	1.0 M KOH	η_{100}=346	79.3	Ni foam	[13]
Ni_3S_2-Co_9S_8 nanowires	1.0 M KOH	η_{20}=294 η_{50}=320 η_{100}=350	80	Ni foam	[14]
Co_9S_8-Ni_3S_2 nanotubes	1.0 M KOH	η_{50}=281	53.3	Ni foam	[15]
Ni_3S_2/Co_9S_8	1.0 M KOH	η_{100}=340	66	Ni foam	[16]
SnS-Ni_3S_2/NF	1.0 M KOH	η_{100}=387	126	Ni foam	[17]
NiCo-LDH/$NiCo_2S_4$ /CC	1.0 M KOH	η_{100}=254	48	CC	[18]

Ni_3S_2/FeS	1.0 M KOH	η_{30}=295	79.8	-	[19]
Co9S8/Cu2S/CF	1.0 M KOH	η_{10}=195 η_{50}=255	78.8	Cu foam	[20]
Fe,Mn-Ni_3S_2/NF	1.0 M KOH	η_{30}=216	63.29	Ni foam	[21]
Ni_3S_2@MIL-53 (NiFeCo)	1.0 M KOH	η_{50}=236	14.8	Ni foam	[22]
Ni_3S_2-CeO_2	1.0 M KOH	η_{20}=264	146	Ni foam	[23]
NiO- Ni_3S_2	1.0 M KOH	η_{20}=290	75	Ni foam	[24]
Ni_3S_2/NiS hollow core	1.0 M KOH	η_{10}=298	58.6	-	[25]
MoS_2/NiS	1.0 M KOH	η_{10}=350	108	-	[26]
NiS/Bi_2WO_6	1.0 M KOH	η_{10}=527	238	-	[27]
Ni_3S_2/Ni@CC	1.0 M KOH	η_{10}=290.9	101.26	CC	[28]
$FeNi_3N$- Ni_3S_2	1.0 M KOH	η_{10}=230	38	-	[29]
N- Ni_3S_2/VS_2	1.0 M KOH	η_{10}=227	60	-	[30]
Ni- Ni_3S_2@carbon	1.0 M KOH	η_{10}=284	56	-	[31]
Co/Ce- Ni_3S_2	1.0 M KOH	η_{20}=286	71.7	Ni foam	[32]
Ni_3S_2/MIL-53(Fe)	1.0 M KOH	η_{10}=214 η_{100}=251	33.8	-	[33]
CoS_2/ Ni_3S_2/$CoNiO_x$	1.0 M KOH	η_{10}=256 η_{100}=300	43.4	-	[34]
$Fe_{7.2\%}$- Ni_3S_2 NSs	1.0 M KOH	η_{10}=295	71	Ni foam	[35]
S- Ni_3S_2	1.0 M KOH	η_{10}=213 η_{100}=286	45	-	[36]
NiFe-Co_9S_8	1.0 M KOH	η_{10}=219	55	CC	[37]
NiS/NiS_2	1.0 M KOH	η_{100}=416	156.5	-	[38]

Table S3. EIS results of W-Ni_3S_2/Ni_7S_6, W-Ni_3S_2, Ni_3S_2, Ni_7S_6 and NF.

catalyst	Solution series resistances R_s (Ω)	Charge transfer resistance R_{ct} (Ω)
Ni_3S_2	1.972	5.709
Ni_7S_6	1.957	6.282
W-Ni_3S_2	1.892	1.498
W-Ni_3S_2/Ni_7S_6	1.988	0.7334

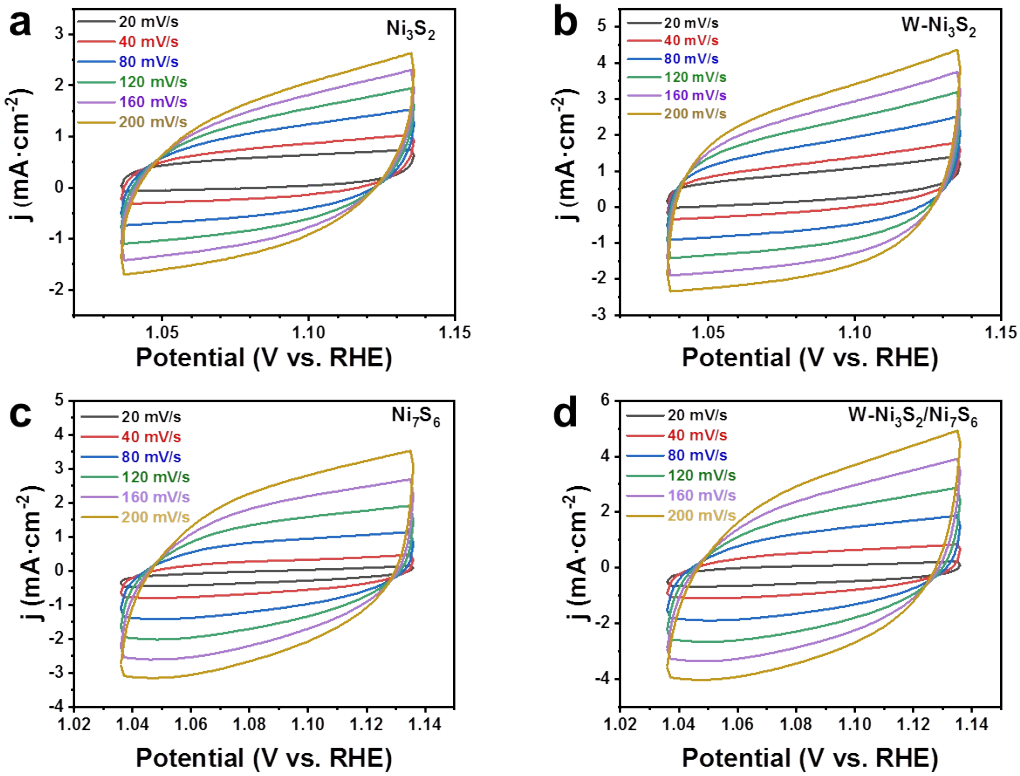

Figure S9. CV plots of a) Ni_3S_2, b) W-Ni_3S_2, c) Ni_7S_6, d) W-Ni_3S_2/Ni_7S_6 at different scan rates.

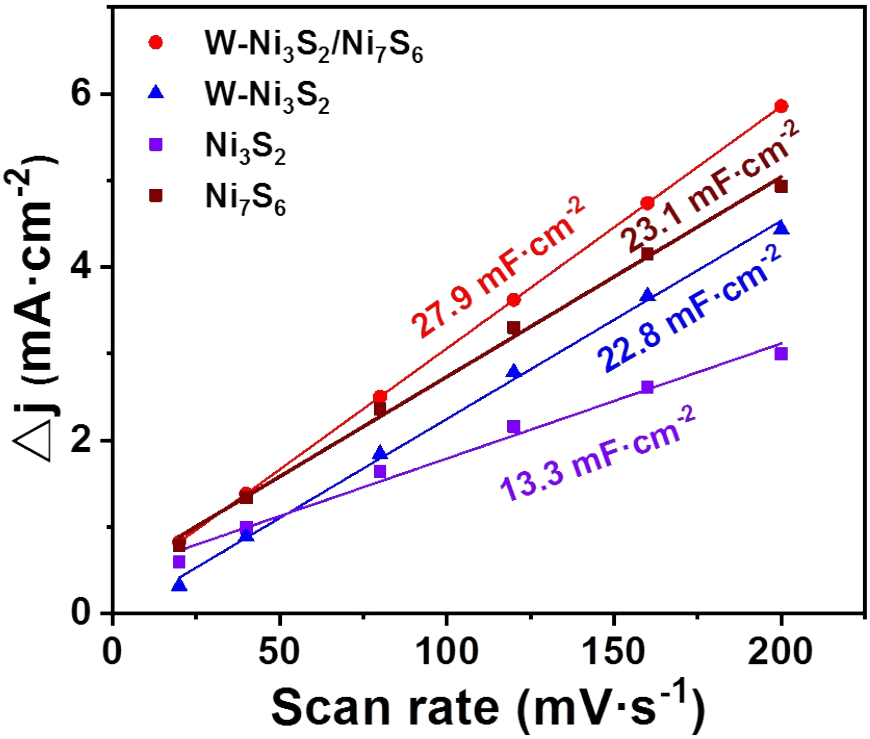

Figure S10. Capacitive currents as a function of the scan rate to give the double-layer capacitance (C_{dl}) for different catalysts.

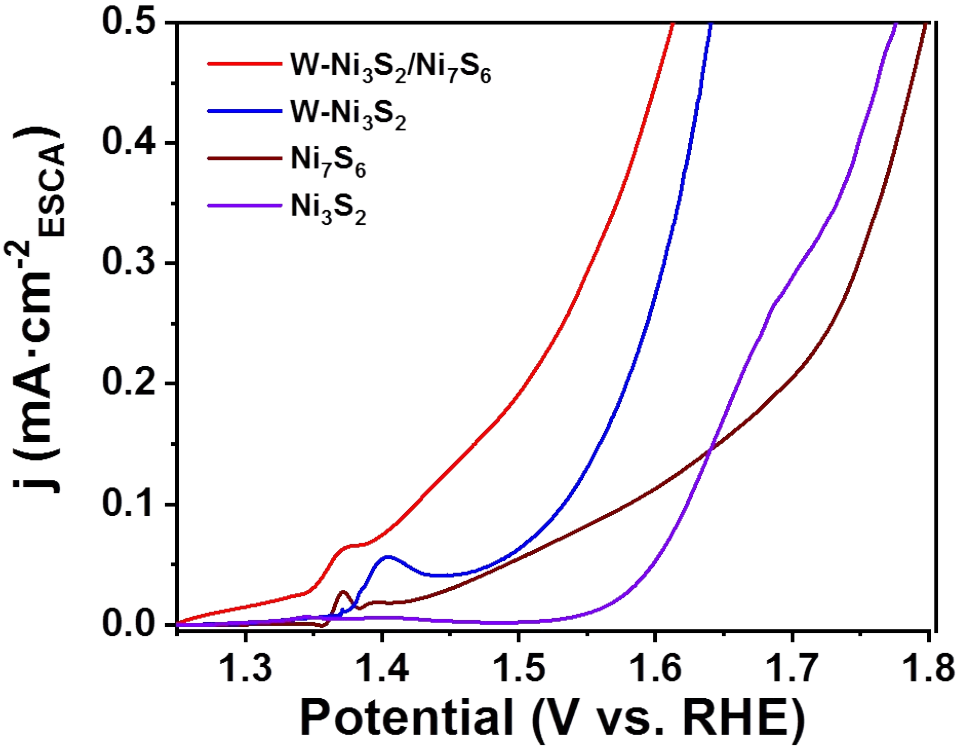

Figure S11. The OER performance of Ni_3S_2, W-Ni_3S_2 and W-Ni_3S_2/Ni_7S_6 after the electrochemical surface area normalization.

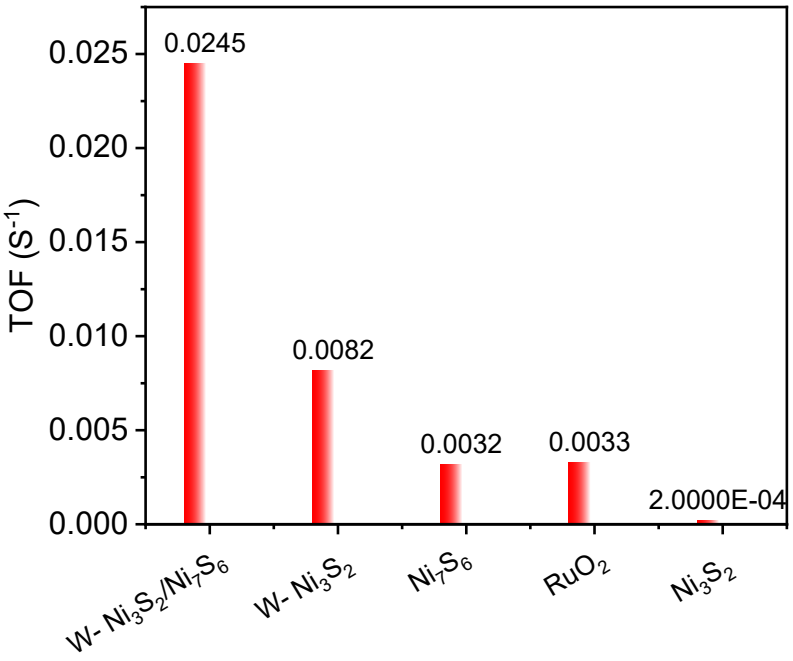

Figure S12. TOF of different electrocatalysts at an overpotential of 300 mV.

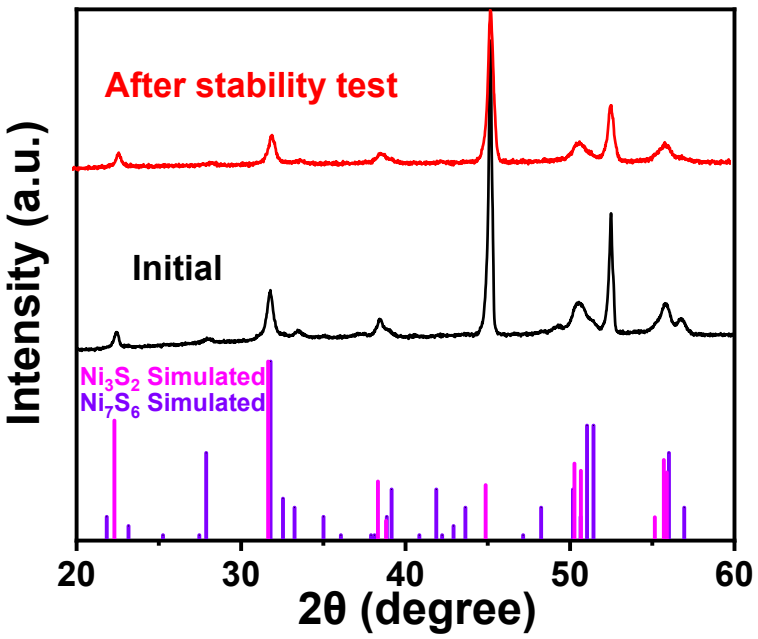

Figure S13. XRD patterns of W-Ni_3S_2/Ni_7S_6 before and after stability test.

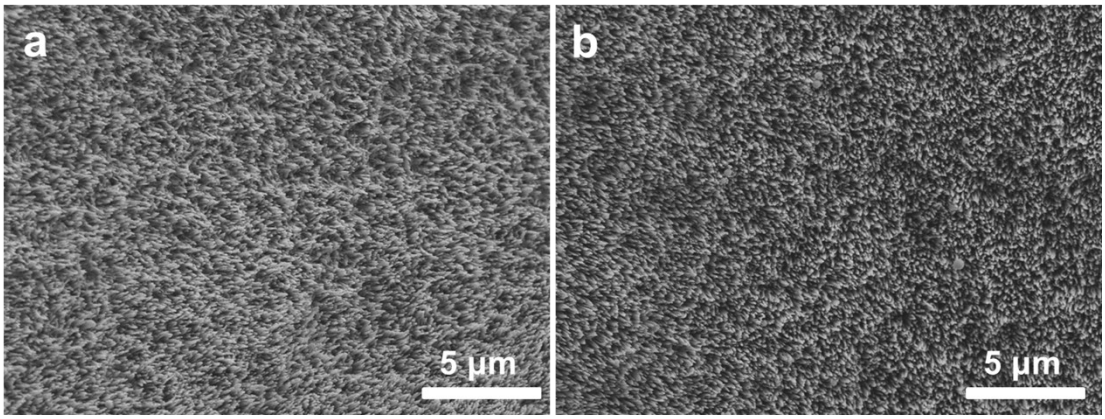

Figure S14. SEM images of W-Ni_3S_2/Ni_7S_6 a) before and b) after stability test.

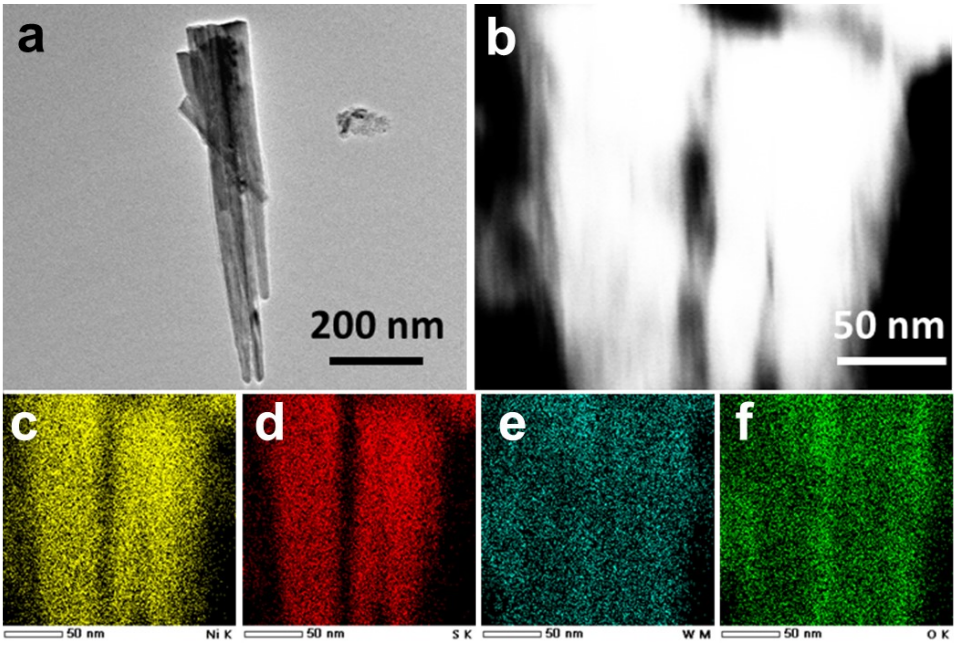

Figure S15. a) TEM images b) HRTEM images c–f) HAADF-STEM images of the W-Ni_3S_2/Ni_7S_6 after stability test.

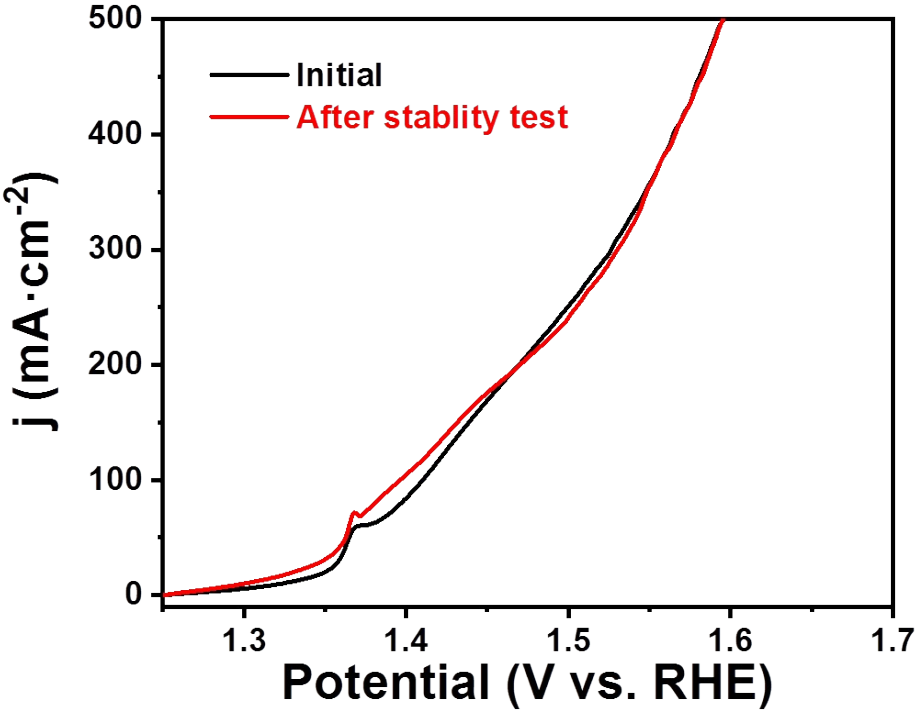

Figure S16. OER performances of W-Ni_3S_2/Ni_7S_6 before and after stability test in 1.0 M KOH.

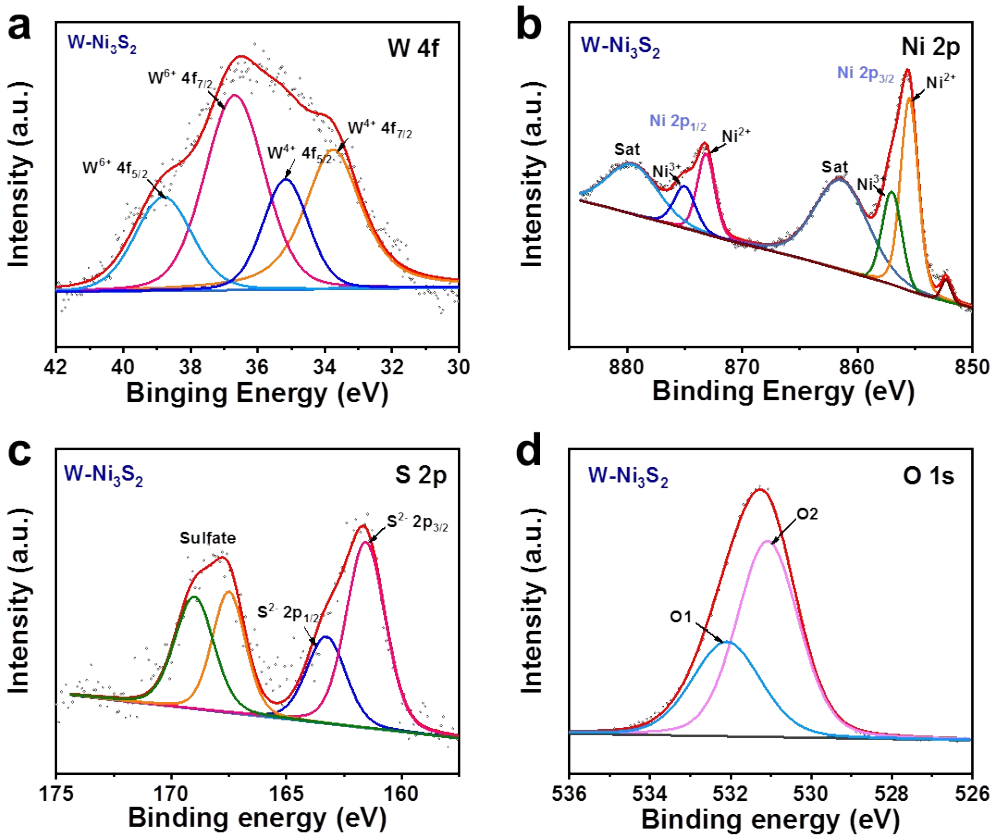

Figure S17. a) W 4f XPS spectra, b) Ni 2p XPS spectra, c) S 2p XPS spectra, d) O 1s XPS spectra of W-Ni_3S_2.

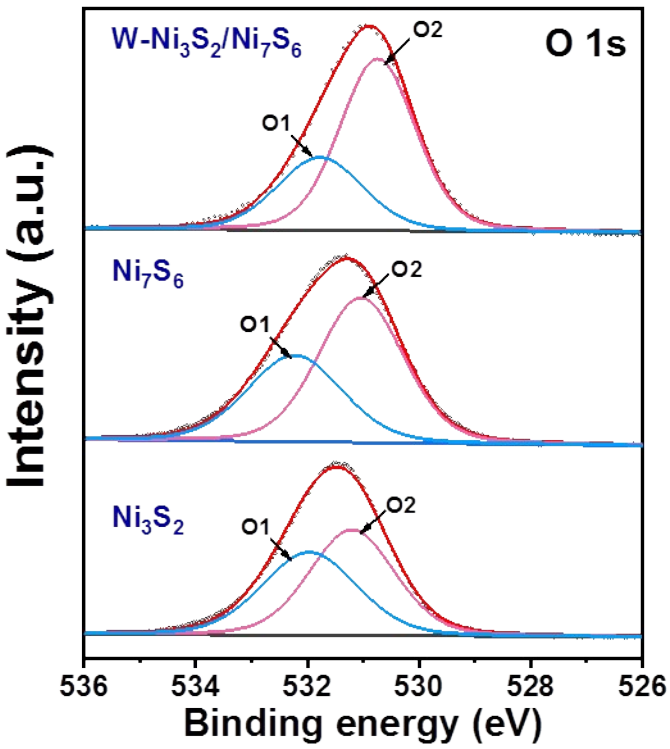

Figure S18. O 1s XPS spectra of Ni_3S_2, Ni_7S_6 and W-Ni_3S_2/Ni_7S_6.

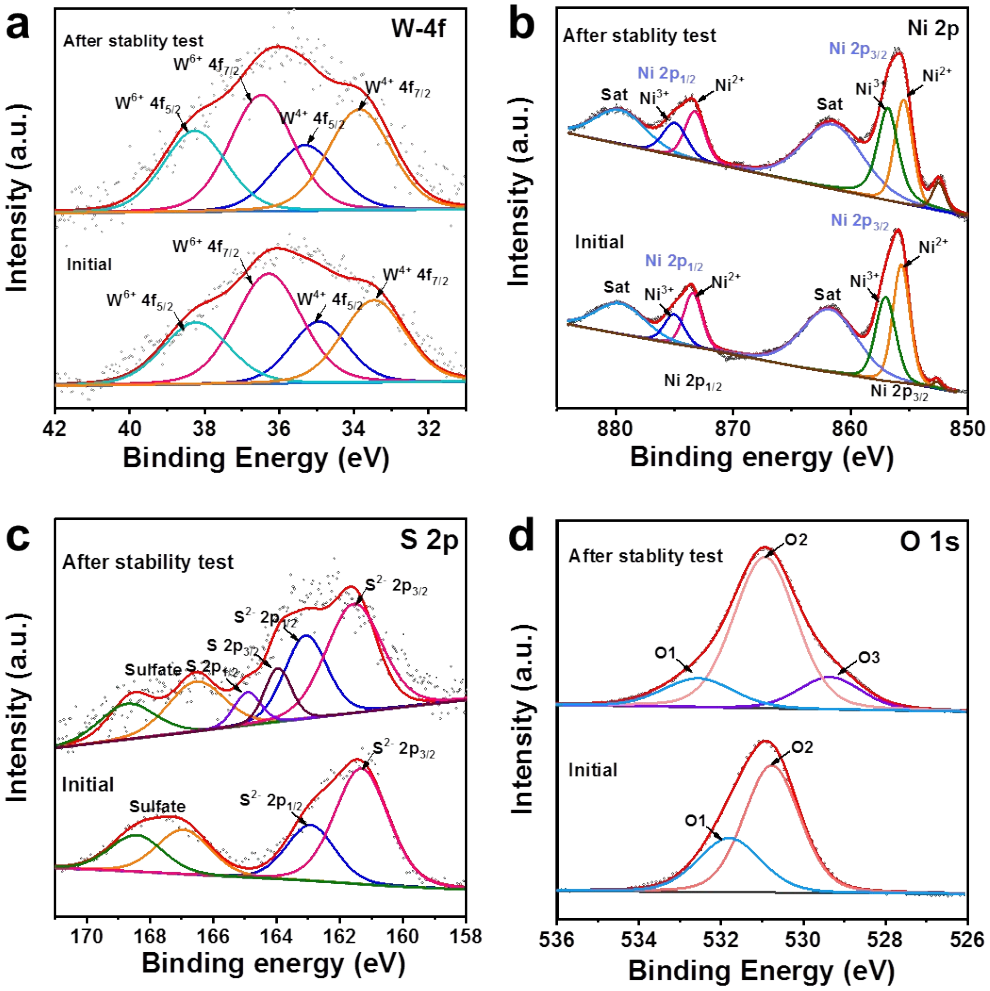

Figure S19. a) W 4f XPS spectra, b) Ni 2p XPS spectra, c) S 2p XPS spectra, d) O 1s XPS spectra of W-Ni_3S_2/Ni_7S_6 before and after stability test in 1.0 M KOH.

[1] Z. Xue, Y. Li, Y. Zhang, W. Geng, B. Jia, J. Tang, S. Bao, H. Wang, Y. Fan, Z. Wei, Z. Zhang, Z. Ke, G. Li, C. Su, *Advanced Energy Materials*. **2018**, 8, 1801564.

[2] G. Ren, Q. Hao, J. Mao, L. Liang, H. Liu, C. Liu, J. Zhang, *Nanoscale*. **2018**, 10, 17347.

[3] B. Fei, Z. Chen, J. Liu, H. Xu, X. Yan, H. Qing, M. Chen, R. Wu, *Advanced Energy Materials*. **2020**, 10, 2001963.

[4] Y. Yang, H. Yao, Z. Yu, S. M. Islam, H. He, M. Yuan, Y. Yue, K. Xu, W. Hao, G. Sun, H. Li, S. Ma, P. Zapol, M. G. Kanatzidis, *Journal of the American Chemical Society*. **2019**, 141, 10417.

[5] X. Luo, P. Ji, P. Wang, R. Cheng, D. Chen, C. Lin, J. Zhang, J. He, Z. Shi, N. Li, S. Xiao, S. Mu, *Advanced Energy Materials*. **2020**, 10, 1903891.

[6] C. Hu, L. Zhang, Z. Zhao, A. Li, X. Chang, J. Gong, *Advanced Materials*. **2018**, 30, 1705538.

[7] J. Dong, F. Zhang, Y. Yang, Y. Zhang, H. He, X. Huang, X. Fan, X. Zhang, *Applied Catalysis B: Environmental*. **2019**, 243, 693.

[8] P. Hua, Z. Jia, H. Che, W. Zhou, N. Liu, F. Li, J. Wang, *Journal of Power Sources*. **2019**, 416, 95.

[9] K. Feng, D. Zhang, F. Liu, H. Li, J. Xu, Y. Xia, Y. Li, H. Lin, S. Wang, M. Shao, Z. Kang, J. Zhong, *Advanced Energy Materials*. **2020**, 10, 2000184.

[10] Z. Wang, Z. Lin, J. Deng, S. Shen, F. Meng, J. Zhang, Q. Zhang, W. Zhong, L. Gu, *Advanced Energy Materials*. **2021**, 11, 2003023.

[11] X. Du, P. Che, Y. Wang, C. Yuan, X. Zhang, *International Journal of Hydrogen Energy*. **2019**, 44, 22955.

[12] B. Ma, X. Guo, X. Zhang, Y. Chen, X. Fan, Y. Li, F. Zhang, G. Zhang, W. Peng, *Energy Technology*. **2019**, 7, 1900063.

[13] Y. Zhou, S. Xi, X. Yang, H. Wu, *Journal of Solid State Chemistry*. **2019**, 270, 398.

[14] R. Zhang, L. Cheng, Z. Wang, F. Kong, Y. Tsegazab, W. Lv, W. Wang, *Applied Surface Science*. **2020**, 526, 146753.

[15] J. Li, P. Xu, R. Zhou, R. Li, L. Qiu, S. P. Jiang, D. Yuan, *Electrochimica Acta*. **2019**, 299, 152.

[16] J. Lin, H. Wang, X. Zheng, Y. Du, C. Zhao, J. Qi, J. Cao, W. Fei, J. Feng, *Journal of Power Sources*. **2018**, 401, 329.

[17] X. Zang, J. Teng, X. Zhang, J. Guo, *Materials Letters*. **2021**, 287, 129290.

[18] Y. Liu, Y. Bai, W. Yang, J. Ma, K. Sun, *Electrochimica Acta*. **2021**, 367, 137534.

[19] K. Xiao, J. Wei, W. Han, Z. Li, *Journal of Power Sources*. **2021**, 487, 229408.

[20] Z. Zang, X. Wang, X. Li, Q. Zhao, L. Li, X. Yang, X. Yu, X. Zhang, Z. Lu, *ACS Appl Mater Interfaces*. **2021**, 13, 9865.

[21] J. Duan, Z. Han, R. Zhang, J. Feng, L. Zhang, Q. Zhang, A. Wang, *J Colloid Interface Sci*. **2021**, 588, 248.

[22] B. Yuan, C. Li, L. Guan, K. Li, Y. Lin, *Journal of Power Sources*. **2020**, 451, 2003023.

[23] Q. Wu, Q. Gao, L. Sun, H. Guo, X. Tai, D. Li, L. Liu, C. Ling, X. Sun, *Chinese Journal of Catalysis*. **2021**, 42, 482.

[24] L. Peng, J. Shen, X. Zheng, R. Xiang, M. Deng, Z. Mao, Z. Feng, L. Zhang, L. Li, Z. Wei, *Journal of Catalysis*. **2019**, 369, 345.

[25] J. Wang, H. C. Zeng, *ACS Applied Materials & Interfaces*. **2019**, 11, 23180.

[26] Q. Qin, L. Chen, T. Wei, X. Liu, *Small*. **2019**, 15, 1803639.

[27] J. Li, X. Xu, B. Zhang, W. Hou, S. Lv, Y. Shi, *Applied Surface Science*. **2020**, 526, 146718.

[28] H. Qian, B. Wu, Z. Nie, T. Liu, P. Liu, H. He, J. Wu, Z. Chen, S. Chen, *Chemical Engineering Journal*. **2020**, 420, 127646.

[29] S. Liang, M. Jing, E. Pervaiz, H. Guo, T. Thomas, W. Song, J. Xu, A. Saad, J. Wang, H. Shen, J. Liu, M. Yang, *ACS Applied Materials & Interfaces*. **2020**, 12, 41464.
[30] X. Zhong, J. Tang, J. Wang, M. Shao, J. Chai, S. Wang, M. Yang, Y. Yang, N. Wang, S. Wang, B. Xu, H. Pan, *Electrochimica Acta*. **2018**, 269, 55.
[31] Y. Lin, G. Chen, H. Wan, F. Chen, X. Liu, R. Ma, *Small*. **2019**, 15, 1900348.
[32] X. Wu, T. Zhang, J. Wei, P. Feng, X. Yan, Y. Tang, *Nano Research*. **2020**, 13, 2130.
[33] F. Wu, X. Guo, Q. Wang, S. Lu, J. Wang, Y. Hu, G. Hao, Q. Li, M.-Q. Yang, W. Jiang, *Journal of Materials Chemistry A*. **2020**, 8, 14574.
[34] H. Lee, X. Wu, Q. Ye, X. Wu, X. Wang, Y. Zhao, L. Sun, *Chemical Communications*. **2019**, 55, 1564.
[35] Y. Zhu, H. Yang, K. Lan, K. Iqbal, Y. Liu, P. Ma, Z. Zhao, S. Luo, Y. Luo, J. Ma, *Nanoscale*. **2019**, 11, 2355.
[36] H. Zhang, H. Jiang, Y. Hu, Y. Li, Q. Xu, S. Petr, C. Li, *Journal of Materials Chemistry A*. **2019**, 7, 7548.
[37] C. Zhan, Z. Liu, Y. Zhou, M. Guo, X. Zhang, J. Tu, L. Ding, Y. Cao, *Nanoscale*. **2019**, 11, 3378.
[38] Q. Li, D. Wang, C. Han, X. Ma, Q. Lu, Z. Xing, X. Yang, *Journal of Materials Chemistry A*. **2018**, 6, 8233.